

submitted to *J. Mater. Chem.*, MD2 ms# 9/05196A  
revised  
in press

28.6.1999  
28.7.1999

## Coupling of protein sheet crystals (S-layers) to phospholipid monolayers

Markus Weygand,<sup>a</sup> Manfred Schalke,<sup>a</sup> Paul B. Howes,<sup>b,d</sup> Kristian Kjaer,<sup>b</sup> Jaqueline Friedmann,<sup>c</sup>  
Barbara Wetzer,<sup>c,e</sup> Dietmar Pum,<sup>c</sup> Uwe B. Sleytr,<sup>c</sup> and Mathias Loesche<sup>a,\*</sup>

<sup>a</sup>Leipzig University, Institute of Experimental Physics I, D-04103 Leipzig, Germany.

E-mail: loesche@physik.uni-leipzig.de

<sup>b</sup>Risø National Laboratory, Department of Solid State Physics and Chemistry, DK-4000 Roskilde, Denmark

<sup>c</sup>University for Agricultural Sciences, Center for Ultrastructure Research and Ludwig-Boltzmann-Institute for Molecular Nanotechnology, A-1180 Vienna, Austria

<sup>d</sup>Current address: University of Leicester, Department of Physics and Astronomy, Leicester LE17RH, U. K.

<sup>e</sup>Current address: Rhône-Poulenc Rorer, F-94403 Vitry-sur-Seine, France

### ABSTRACT

The coupling of bacterial S-layer proteins to phospholipid membranes has been studied in molecular details with respect to, particularly, the lipid headgroups. Emphasis has been laid on two of the best characterized protein species, the S-layer protein from *Bacillus sphaericus* CCM2177 and from *Bacillus coagulans* E38-66/V1. A combination of fluorescence microscopy, surface sensitive scattering techniques (grazing-incidence X-ray diffraction as well as X-ray and neutron reflectometry) and infrared spectroscopy (FT-IRRAS), applied to surface monolayers of lipids onto which the protein has been reconstituted as continuous molecular crystal sheets, provides a wealth of information which has been utilized to propose detailed molecular models.

---

\* To whom correspondence should be addressed

## INTRODUCTION

Protein/lipid interactions play an important role in life science. In biomimetic approaches to materials science, well-defined proteinaceous interface layers gain progressively more importance in various fields, such as biosensorics,<sup>1</sup> biocatalysis,<sup>2</sup> and the build-up of well-defined supramolecular architectures at interfaces.<sup>3,4</sup> Since a large variety of biological processes is membrane mediated, there is great interest in the meso- and macroscopic reconstitution of functional lipid membranes.<sup>5</sup> On the other hand, the use of free-standing membranes is primarily impeded by a low stability. It was recently demonstrated that the stability of such membranes can be significantly increased by the recrystallization of isolated S-layer proteins. Such composite S-layer/lipid films are biomimetic structures which resemble those archaeal cell envelopes that are exclusively composed of monomolecular arrays of (glyco)proteins and a closely associated plasma membrane.<sup>6</sup> Bacterial and archaeal surface layers (S-layers) are monomolecular protein sheet crystals covering the outer surface of prokaryotic organisms.<sup>7,8</sup> They constitute the outermost component of such cells providing mechanical support to the cell in Archaeae and control material transfer from and into the cell as their crystal lattice incorporates pores. Most S-layers consist of one single protein (or glycoprotein) species that is specific for the organism it derives from. While S-layer proteins reassemble into sheet crystals under a variety of experimental conditions, three-dimensional crystallization has not been achieved to date for any protein of this class such that atomic level structural information is not at hand. On the molecular scale, the topographical properties of S-layers and in particular the topography of the S-layer lattice from *B. coagulans* E38–66/V1 have been revealed by electron microscopy.<sup>7</sup> The structural properties of the S-layers from various organisms may vary greatly<sup>7,10</sup> ( $M_r$  between  $\sim 40,000$  and  $\sim 200,000$ ; lattice constants between  $\sim 3$  and  $\sim 30$  nm; S-layer thickness between  $\sim 5$  and  $\sim 15$  nm). Other features are quite similar for many of the S-layers studied so far: Protein within the S-layer occupies only a fraction of the area, typically 30–70%, such that large water-filled pores span the S-layer. A pronounced asymmetry of the topographical and physico-chemical properties of the two faces oriented to the cell wall („inner face“) or pointing away to the environment („outer face“) has been observed for various S-layer species: The inner surfaces are generally more corrugated than the outer ones and bear net negative charges.<sup>11</sup> The overall amino acid composition is similar for many species studied to date, with a high abundance of glutamic and aspartic acid and little or no sulfur-containing amino acids.<sup>7,12</sup> In Gram-positive bacteria, such as the ones studied in this paper, the S-layer is associated with the peptidoglycane-containing cell wall, but *not* with a cytoplasmatic membrane as in most archaeae.

While they are *in vivo* attached to cell walls, S-layer proteins isolated from *Bacillus coagulans* E38–66/V1 and *B. sphaericus* CCM2177 are rather easy to recrystallize at a large variety of interfaces – including lipid surfaces.<sup>13</sup> With the goal to use such reconstituted S-layers for the stabilization of model membranes, we have investigated the – unnatural – association and recrystallization of these two protein species at phospholipids. Recrystallized S-layers, particularly of the protein derived from *B. coagulans* E38–66, may cover holes several microns large, and larger areas of phospholipid films have been observed to be overgrown by molecularly thin polycrystal films.<sup>14-16</sup> We have demonstrated that the attachment of monomolecular protein sheet crystals stabilize the fragile lipid double layer in membrane models used for biophysical studies.<sup>17,18</sup> Since S-layers are natural molecular sieves with a well-defined porosity, such an attached protein sheet crystal does not inhibit molecular diffusion processes to the membrane and allows for manipulation of the membrane model. In order to understand the interaction and the coupling between protein and lipid in molecular detail, we have set out to investigate such molecular hetero-layer systems with a variety of surface sensitive characterization techniques including fluorescence microscopy, X-ray and neutron scattering, and FTIR spectroscopy.

## MATERIALS AND METHODS

*Bacillus sphaericus* (*B. sphaericus*) strain CCM2177 was obtained from the Czech Collection of Microorganisms (Brno, Czech Republic). *B. coagulans* E38–66/V1 was from F. Hollaus (Zuckerforschung Tulln GmbH, Tulln, Austria). Growth conditions of the bacteria in continuous culture were as reported,<sup>19</sup> and extraction of the S-layer protein with guanidine hydrochloride (GHCl, 5 M in 50mM Tris-HCl buffer, pH 7.2, 20°C) was performed as described.<sup>19</sup> GHCl extracts were dialyzed against H<sub>2</sub>O (*B. sphaericus*) or 10 mM CaCl<sub>2</sub> (*B. coagulans*). Dipalmitoylphosphatidylethanolamine (DPPE), dimyristoylphosphatidylethanolamine (DMPE) and dipalmitoylphosphatidylcholine (DPPC) were purchased from Avanti Polar Lipids, Inc. (Birmingham, AL) and used as received. Lipids were dissolved in CHCl<sub>3</sub>/CH<sub>3</sub>OH (3:1, Merck, Darmstadt, Germany, *pro analysi* grade) to form a spreading solution of ~ 1.0 mg/ml. Ultrapure H<sub>2</sub>O was prepared by filtering in a Milli-Q (Millipore, Bedford, MA) apparatus. For a translation of the scattering length density profiles obtained in reflectivity experiments (see below) into mass density, the amino acid composition of the proteins has been determined.<sup>12</sup>

All experiments were performed at room temperature ( $T = 21 \pm 1^\circ\text{C}$ ). Self-assembly products of the purified S-layer proteins were sedimented at  $40,000 \times g$  and  $T = 4^\circ\text{C}$  immediately before use. The

clear supernatant containing protein monomers in a concentration of typically 2 mg/ml was injected underneath phospholipid monolayers preformed at the desired lateral pressure  $\pi$ . In typical experiments,  $\pi$  was observed to increase slightly after protein injection, e.g. by a few mN/m.<sup>16</sup> The protein was allowed to recrystallize over night for most of the experiments reported here.

Fluorescence microscopy for the observation of molecular protein/lipid layer systems at aqueous surfaces has been described in detail.<sup>20</sup> For dual label experiments, the S-layer protein from *B. coagulans* was labeled with carboxyfluorescein (CFS) as described<sup>20</sup> and was observed in conjunction with phospholipid surface monolayers that contained  $\sim 2$  mol% of a sulforhodamin- (SR-) labeled DPPE. By means of the different labels, structure formation in the protein and lipid layers may be well discriminated.

X-ray reflectivity and diffraction (grazing-incidence X-ray diffraction, GIXD) experiments were performed at the BW1 beam line of HASYLAB (DESY, Hamburg, Germany).<sup>21</sup> In addition, x-ray reflection measurements in a more confined momentum transfer regime were taken on a laboratory scale instrument in Leipzig.<sup>22</sup> Neutron reflectometry was done at the new Mark II instrument, equipped with Langmuir-type liquid surface sample cell, at port TAS9 in the guide hall of the DR3 reactor at Risø National Laboratory (Roskilde, Denmark). All surface scattering experiments were performed using home-built Langmuir film balances (surface area  $16 \times 30$  cm<sup>2</sup>) incorporated in gas-tight, thermostated Al containers with Kapton (X-ray) or Al (neutron experiments) windows for the beam.<sup>23</sup> Polished ( $\lambda/10$ ) Pyrex (boron silicate) glass blocks, inserted into the subphases to diminish the depth under the beam footprint on the monolayer to  $\sim 300$   $\mu$ m, were used to suppress surface waves in the film balances.

Reflectivity data were interpreted in terms of a model-free constrained least-squares approach introduced by Skov Pedersen and Hamley<sup>24-26</sup> where the scattering length density distribution  $\rho(z)$  across the interface is described by B-spline functions:

$$\rho(z) = \sum_{i=1}^N a_i B_i(z) \quad (1)$$

Here,  $z$  indicates the direction of the surface normal – whereas  $x$  and  $y$  define the area of the aqueous surface – and  $N$  is determined by the accessible  $Q_z$ -range via the sampling theorem.  $\rho(z)$  is determined in a constrained least-squares fit that aims at suppressing solutions with large oscillations in  $\rho$ .

As a function of the horizontal component  $Q_{xy} \sim \left(4\pi/\lambda\right) \sin(2\theta_{xy}/2)$  of the scattering vector, the

intensity diffracted from 2D crystal patches peaks at Bragg positions  $Q_{xy}^{hk}$ . In the absence of a crystalline repeat in the vertical ( $z$ ) direction, the intensity extends as a smooth function, the Bragg rod profile  $I_{hk}(Q_z)$ , of the vertical component of the scattering vector,  $Q_z \sim \left(2\pi/\lambda\right)\sin(\alpha_f)$ , where  $\alpha_f$  is the vertical direction of the scattered rays. The Bragg rod profiles resulting from the phospholipid chains may be modeled<sup>27,28</sup> by

$$I_{hk}(Q_z) = \sum_{(hk)} |V(\alpha_f)|^2 \times \text{sinc}^2 \left[ \frac{1}{2} L \left( Q_z \cos \vartheta - \left( \mathbf{Q}_{xy}^{hk} \cdot \hat{\mathbf{e}} \right) \sin \vartheta \right) \right] \times \exp(-Q_z^2 \sigma^2) \quad (2),$$

where  $|V|^2$  is the Yoneda-Vineyard peak,<sup>29</sup>  $L$  is the length of the palmitoyl chains,  $\hat{\mathbf{e}}$  is a horizontal unit vector defining the tilt azimuth,  $\mathbf{Q}_{xy}^{hk}$  is the in-plane reciprocal lattice vector,  $\sigma$  is the vertical r.m.s. displacement, and the sum is over all Bragg reflections contributing to the intensity at the position  $Q_{xy}^{hk}$ . From Eq. (2) it follows<sup>30</sup> that for each peak (h,k) the coordinates  $\mathbf{Q}_{xy}^{hk}$  and  $Q_z^{hk}$  are related by

$$Q_z^{hk} = \left( \mathbf{Q}_{xy}^{hk} \cdot \hat{\mathbf{e}} \right) \tan \vartheta \quad (3),$$

where  $J$  is the tilt angle of the chains measured from the surface normal. For well resolved peaks,  $J$  and the azimuthal direction  $\hat{\mathbf{e}}$  can be deduced directly from the set of Eqs. (3).

Infrared reflection-absorption spectroscopy (FT-IRRAS) measurements<sup>31,32</sup> were performed with a Bio-Rad (Digilab) FTS 60A spectrometer equipped with an MCT detector. The monolayer was spread in a home-made thermostated Langmuir trough that is mounted on a shuttle device together with another trough containing pure water<sup>33</sup> which allows the IR beam to be switched between the sample and a reference area. Spectra were acquired by coaddition of 1024 scans with a resolution of 8  $\text{cm}^{-1}$ .

## MOTIVATION

We have studied the structure formation in lipid monolayer/recrystallized S-layer systems on the mesoscopic length scale with fluorescence microscopy (FM) and electron microscopy (EM). In recent extensive EM investigations, we addressed systematically the question, which lipids and which experimental conditions support the recrystallization of the protein from *B. coagulans* E38–66/V1 into well-ordered, coherent S-layers.<sup>16</sup> In older FM and FTIR studies, we have investigated the interplay between order and disorder in the system.<sup>20</sup> In that study, we used a dual label technique to

discriminate between structure formation in a phospholipid (DMPE) monolayer, labeled with small amounts of SR-DPPE and adsorption and recrystallization of CFS-labeled protein. When the phospholipid monolayer, which served as a crystallization matrix for the proteins, was prepared in a phase separated (LE/LC) state,\* it was observed that the protein adsorbed preferentially to those areas in the monolayer that was of lower molecular order with respect to the lipid acyl chains. However, nucleation of protein crystals occurred inevitably at locations on the phase boundaries (*cf.* Fig. 1 a/b of ref. 20). Subsequently, crystallization was only observed to occur underneath the ordered lipid phase (*cf.* Fig. 1 e/f of ref. 20). Only after long incubation times did we observe S-layers that had overgrown the entire surface area, i.e., protein crystals that were attached to areas covered by both ordered and disordered lipid. On the other hand, FTIR spectra of the acyl methylene vibrations indicated an increase in the (average) order parameter, which suggests that the association of protein with disordered lipid has been driving the lipid chains into a state of higher order.<sup>20</sup> The complex interplay between order and disorder in this system is schematically depicted in Fig. 1. From indirect arguments it was postulated that the protein upon attachment to the lipid-covered interface is unlikely to interpenetrate into the alkane phase. Rather, it was argued, that the control of the protein crystallization process, which requires information transfer from the lipid to the interface, occurs via the lipid headgroups, and it was hence concluded that the protein is likely to interpenetrate the headgroups – but not the acyl chains – of the lipid monolayer.<sup>20</sup>

In systematic recrystallization experiments, using EM on transferred and stained protein/lipid interface layers, we have addressed the question, which lipid species and which experimental conditions sustain the recrystallization of the S-protein from *B. coagulans* into reconstituted S-layers.<sup>16</sup> It was observed that quite generally disordered lipid acyl chains completely inhibit protein recrystallization at  $\text{pH} > 4$ . It was also found that the chemical identity of the lipid headgroups, as well as divalent cations in the subphase, significantly determine the propensity of the proteins for recrystallization:<sup>16</sup> Anionic lipids on pure water do not support protein recrystallation at all. Underneath zwitterionic lipid headgroups, on the other hand, recrystallization of the protein leads to large S-layer lattices, particularly if  $\text{Ca}^{2+}$  is present in the subphase in mM quantities. Whereas recrystallization at PE interfaces requires  $\text{Ca}^{2+}$ , conceivably to make the headgroups available for protein binding by interrupting the hydrogen-bond network that interlocks the PE groups, proteins recrystallize readily at PC interfaces with or without  $\text{Ca}^{2+}$ .<sup>16</sup> While  $\text{Ca}^{2+}$  induces protein recrystallization even underneath anionic lipids if their

---

\*Phospholipid phases are denoted according to Cadenhead et al.<sup>34</sup>

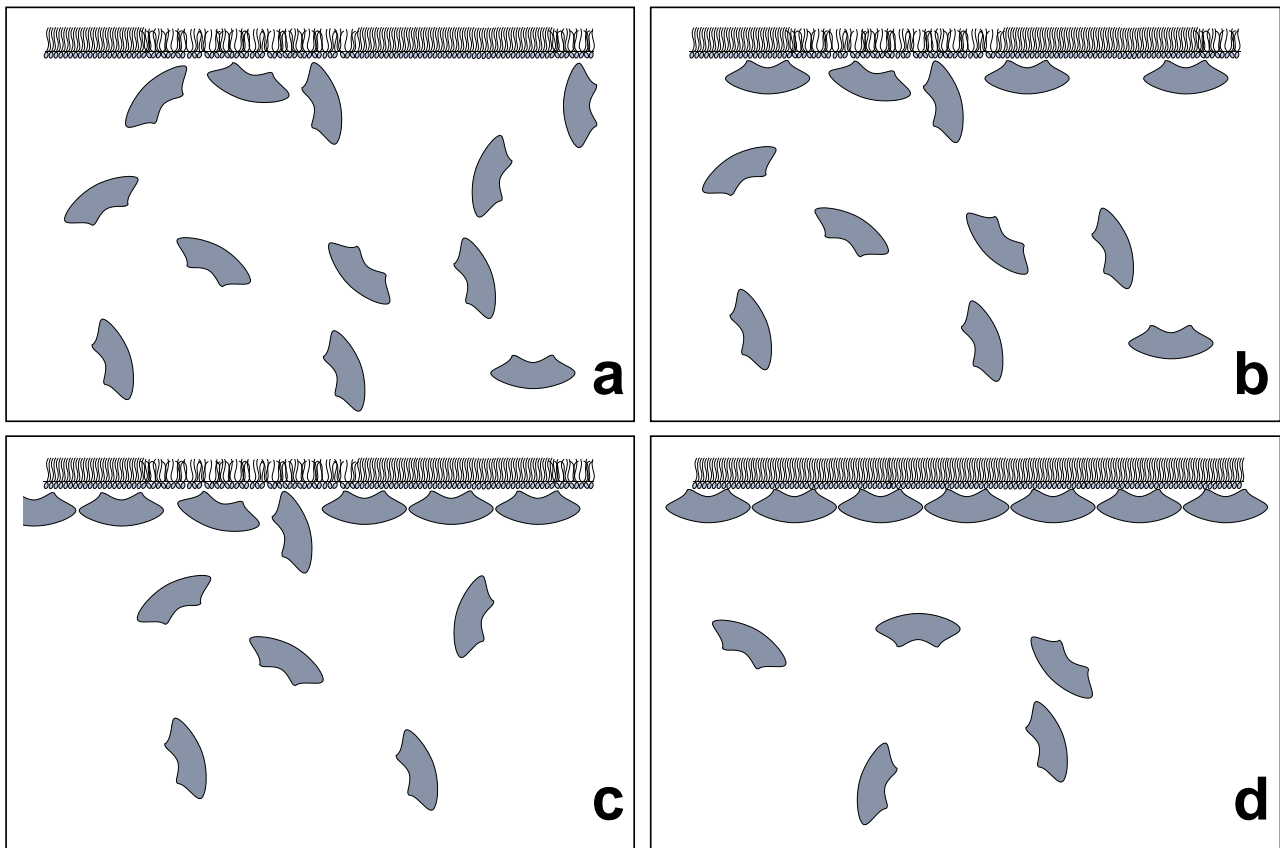


**Figure 1:**

Schematic representation of the adsorption and recrystallization of S-layer protein monomers from Gram-positive bacteria at phospholipid monolayers as it emerges from fluorescence microscopic studies. (a) Protein monomers injected into the subphase underneath a monolayer that has been prepared in a phase separated (LE/LC) state adsorb preferentially to the more disordered LE phase. (b) Nucleation of protein sheet crystals occurs at the LE/LC phase boundary and (c) protein recrystallization proceeds specifically underneath the ordered lipid phase, LC. (d) Only after long incubation times, the reconstituted S-layer covers the entire surface. As evidenced from IR spectroscopy, protein association drives the lipid into a state of higher local order.

headgroups are small (phosphatidic acid, PA), steric repulsion of larger anionic groups (phosphatidylglycerol, PG) inhibits protein attachment to the interface under all experimental conditions. Under a variety of experimental conditions at  $\text{pH} \leq 4.3^*$  and also at clean water surfaces, protein binding and recrystallization is observed in an upside-down orientation, i.e., with the inner face pointing to the subphase compartment. This orientation is distinguished from the „natural“ orientation by virtue of the handedness of the oblique S-layer lattice of this protein.<sup>14</sup> It appears thus<sup>16</sup> that protein binding is determined by anionic sidegroups on the inner surface of the protein, presumably buried in a rugged surface topology that imposes steric constraints on the binding process. Binding of cationic groups to these „primary“ sites occurs in a specific manner in which different lipid headgroups are discriminated against each other. The binding occurs either to partial cationic charges, exposed on the outside region of the lipid headgroups, or to divalent cations which are presumably attached to the phosphate groups, which are located more in the center of the headgroup layer.

\*  $\text{pI} = 4.3$  is the isoelectric point of the S-layer protein from *B. coagulans* E38–66/V1

While these mesoscopic studies yielded a wealth of detailed information, it is important to remember that the molecular scale *interpretation* is rather indirect. We have thus undertaken a study of the S-layer protein interactions with phospholipid interfaces on the microscopic length scale. These investigations are in the focus of the current paper.

## MOLECULAR SCALE STRUCTURE

Figure 2 shows the Bragg reflections, measured in a GIXD experiment, from a quasi-two-dimensional (2D) S-layer lattice formed after incubation of a DPPE monolayer – prepared on an unbuffered subphase containing 10 mM CaCl<sub>2</sub> and compressed to a lateral pressure  $\pi = 28$  mN/m – with the protein from *B. coagulans* E38–66/V1. It shows (panel a) a contour plot of the scattered intensity  $I$  vs. the horizontal and vertical components,  $Q_{xy}$  and  $Q_z$ , of the momentum transfer and (panel b) the  $Q_z$ -integrated intensity vs.  $Q_{xy}$ . The Bragg positions (solid vertical lines) are indexed assuming an oblique lattice with  $|\mathbf{a}| = 99.5$  Å,  $|\mathbf{b}| = 76$  Å, and  $\gamma = 80^\circ$ . For clarity, third order positions (or higher) are shown as broken lines in Fig. 2b only and have not

been labeled. The indexing scheme describes well the observed peak positions for  $Q_{xy} > 0.1 \text{ \AA}^{-1}$ . At lower  $Q_{xy}$ , the coincidence appears worse because of the large sloping background that has not been corrected. The results are consistent with earlier TEM work in which an oblique lattice with  $|\mathbf{a}| = 94$  Å,  $|\mathbf{b}| = 74$  Å, and  $\gamma = 80^\circ$  has been observed.<sup>9,14</sup> Note that the diffraction pattern is quite distinct from the

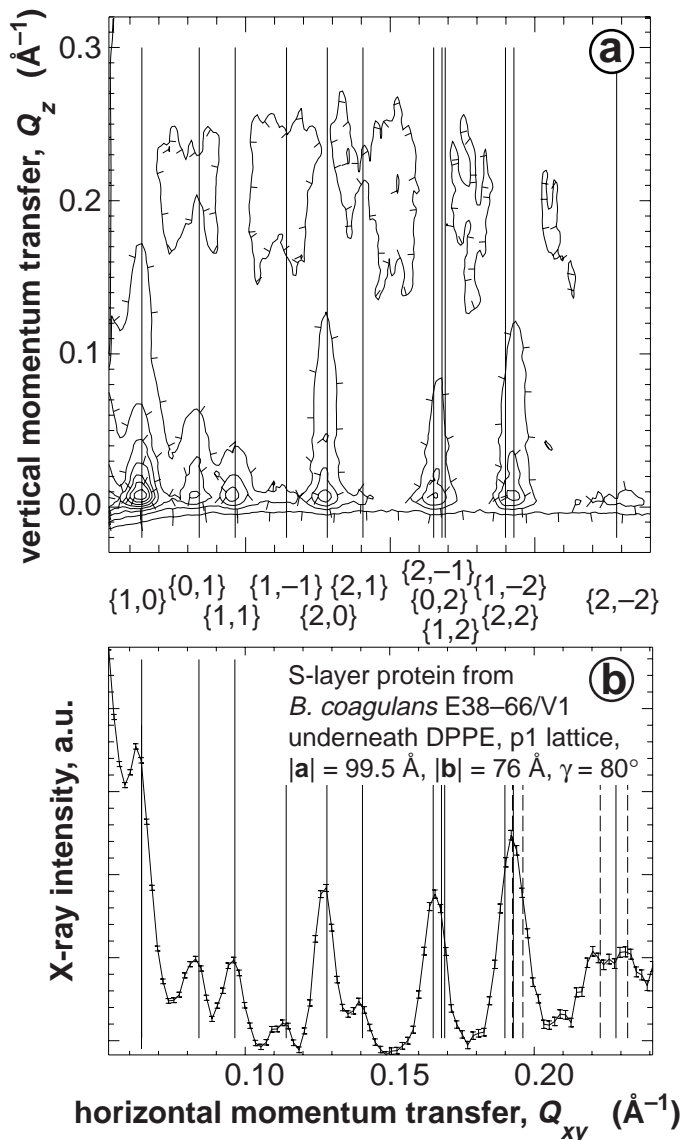


**Figure 2:**

GIXD from an S-layer lattice (*B. coagulans* E38–66/V1) reconstituted underneath a DPPE monolayer. a: Contour plot of the scattered intensity  $I$  vs. the horizontal and vertical components,  $Q_{xy}$  and  $Q_z$ , of the momentum transfer. Note that the intensity as a function of  $Q_{xy}$  is concentrated in Bragg peaks which, vertically resolved, are seen to extend as Bragg rods in the  $Q_z$ -direction. b: The intensity integrated over  $Q_z$  for  $-0.05 < Q_z < 0.45$   $\text{\AA}^{-1}$  is plotted as a function of  $Q_{xy}$ . The vertical lines mark  $Q_{xy}$ -positions of the Bragg maxima corresponding to the indicated  $\{h, k\}$  Miller indices of an oblique lattice with  $|\mathbf{a}| = 99.5$  Å,  $|\mathbf{b}| = 76$  Å and  $\gamma = 80^\circ$ . Dashed lines in (b) indicate third order Bragg positions that have not been labeled.

pattern observed with S-layers from *B. sphaericus* CCM2177, which was earlier studied intensively with surface sensitive scattering techniques.<sup>12</sup> Whereas for S-layers from *B. sphaericus* the scattering intensity is located primarily in the  $\{1,0\}$  and  $\{1,1\}$  peaks in  $Q_z$  positions off the horizon (Fig. 3 of ref. 12), in the case of the S-layer from *B. coagulans* the intensity is concentrated mainly at the horizon ( $Q_z \sim 0$ ) and is more evenly distributed over the various  $\{h,k\}$  peaks.

Independent of the reconstituted S-layer lattice, the order of the lipidic acyl chains may be characterized with GIXD by just tuning to the appropriate  $Q_{xy}$  region.<sup>12</sup> Figure 3 shows the diffraction pattern of a DPPE monolayer on 10 mM  $\text{CaCl}_2$  at  $\pi = 28$  mN/m prior to protein injection (panel a) and after reconstitution of an S-layer from *B. coagulans* (panel c) and (panels b and d) the  $Q_z$ -integrated intensities vs.  $Q_{xy}$ . It is obvious that the phospholipid monolayer undergoes only minimal reorganization upon protein adsorption and recrystallization. A slight increase of the center position of the Bragg peak indicates a lateral compression of the acyl chains on the order of  $\Delta A/A = 1\%$ , where  $A$  is the area per acyl chain in the monolayer. The slight compression of the contour profile of the scattered intensity along  $Q_z$  indicates a marginal reduction of the tilt angle  $\alpha$  of the chains against the surface normal: A quantitative evaluation is consistent with a change from  $\alpha \sim 9^\circ$  to  $6^\circ$ .

As might be expected in view of the remarkable differences between the GIXD patterns of the protein lattices from *B. coagulans* and *B. sphaericus*, the protein density distributions of the two S-layers along the  $z$  direction, as derived from X-ray reflectometry, differ quite drastically. Figure 4 shows a reflectogram of an S-layer reconstituted at a DPPE monolayer on 10 mM  $\text{CaCl}_2$  in comparison

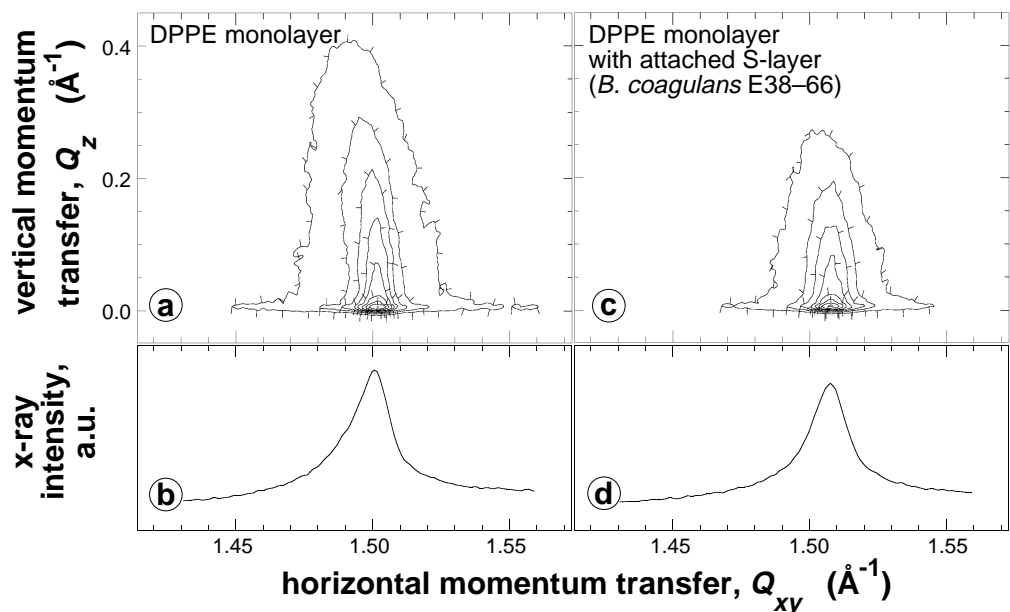


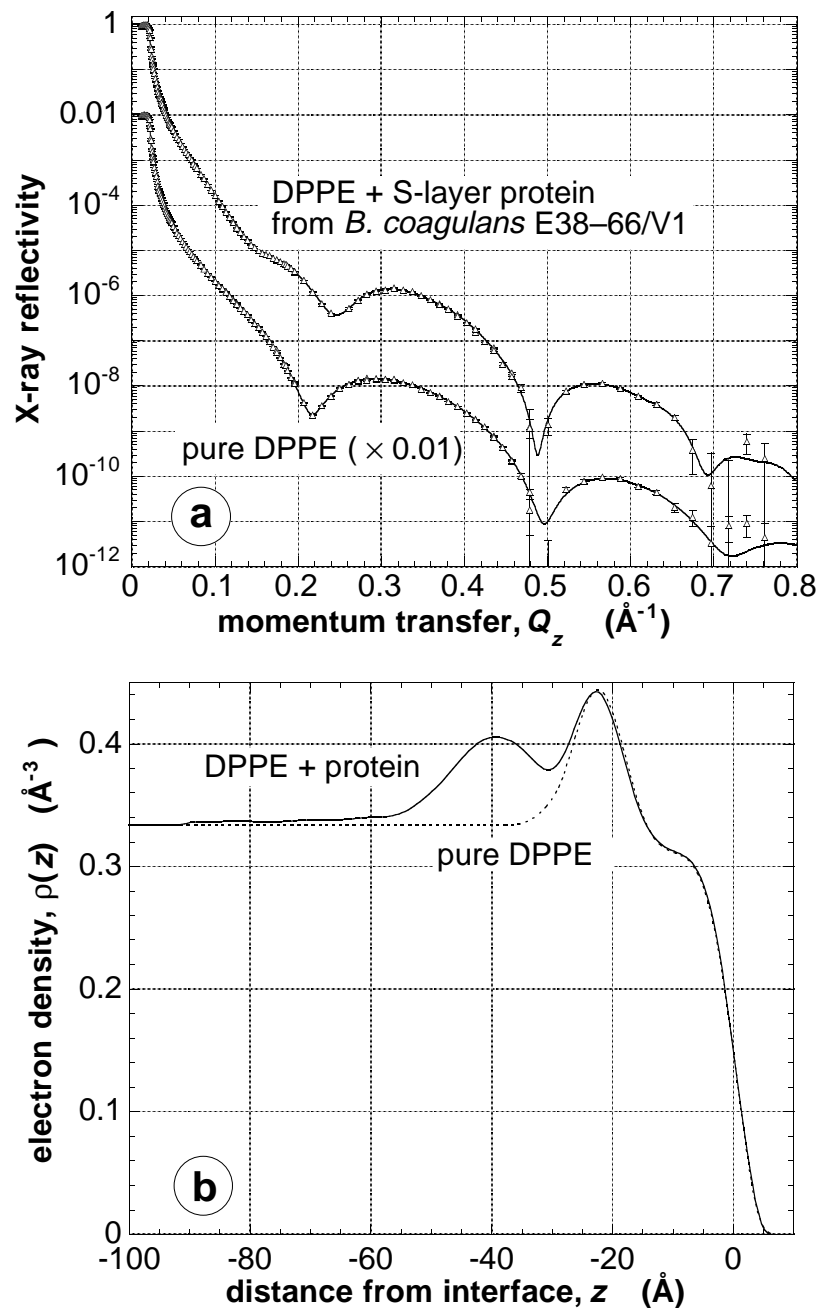
**Figure 3:**

GIXD from a DPPE monolayer at before (a, b;  $\pi \sim 28$  mN/m) and after (c, d;  $\pi \sim 35$  mN/m) adsorption and crystallization of S-layer protein from *B. coagulans* E38–66/V1. The surface area has been kept constant during the S-lattice formation. Top: contour plots of  $I(Q_{xy}, Q_z)$ . Bottom:  $Q_z$ -integrated diffraction intensities  $I(Q_{xy})$ . Adapted from ref. 12.

with that of the DPPE monolayer ( $\pi = 28$  mN/m) prior to protein incubation. The solid lines are the calculated reflectivities corresponding to the electron density models shown in panel b. In earlier work<sup>12</sup> we have shown that the electron density contribution, and hence the volume density, of the S-layer from *B. sphaericus* shows a bimodal distribution that peaks at  $z = -45$  and  $-105$  Å from the surface layer/air interface (corresponding to  $\sim 20$  and  $-80$  Å from the protein/lipid interface) and that the S-layer thickness is  $d_{CCM2177} \sim 90$  Å. This implies that a major part of the protein mass is located close to the outer surface of the S-layer for that bacterial species. In contrast, the data for the *B. coagulans* protein suggest that the center of mass is located close to the S-layer/lipid interface, at  $z \sim -40$  Å from the surface layer/air interface. The outer surface of the S-layer, and thus its thickness, cannot be precisely determined for *B. coagulans* from X-ray reflectometry due to the smooth decay of the electron density contribution of the reconstituted S-layer along the direction into the subphase. The differences in the protein mass density distributions of the two protein species are related to the differences of the diffraction patterns and may explain in qualitative terms why the intensities in the Bragg rods of the diffraction pattern specifically from the reconstituted *B. coagulans* S-layer are concentrated at the horizon.

**Figure 4:**

X-ray reflectivity of a DPPE monolayer prior to and after the reconstitution of an S-layer (*B. coagulans* E38–66/V1). Panel a: Data (open symbols) and models (solid lines) corresponding to the electron density profiles  $\rho(z)$  shown in (b). For clarity, the reflectivity curve of the pure DPPE monolayer (lower trace) has been multiplied by  $10^{-2}$ . In panel (b),  $\rho(z)$  of the pure DPPE monolayer is shown as a dashed line and that of the protein/lipid layer system as a solid line.



Further detail on the interactions between S-layer protein and lipid monolayers is obtained from FT-IRRAS. Figure 5 shows spectra of lipid headgroup vibrations in the range  $\nu = 1,000 \dots 1,300 \text{ cm}^{-1}$ . At least four prominent peaks are identified in this spectral interval: the asymmetric and symmetric phosphate stretch vibrations,  $\nu_{as}(-\text{PO}_2^-)$  and  $\nu_s(-\text{PO}_2^-)$ , around  $1,225$  and  $1,080 \text{ cm}^{-1}$ , respectively, as well as the carbonyl ester vibrations,  $\nu_{as}(-\text{CO}-\text{O}-\text{C}-)$  and  $\nu_s(-\text{CO}-\text{O}-\text{C}-)$ , between  $1,165$  and  $1,180 \text{ cm}^{-1}$  and around  $1,030 \text{ cm}^{-1}$ . Shown in Fig. 5a are spectra from DPPE monolayers without protein on pure water and on  $10 \text{ mM CaCl}_2$  in comparison with a spectrum taken after the reconstitution of an S-layer from *B. coagulans* E38–66/V1. Figure 5b displays spectra involving DPPC. The spectrum of the lipid monolayer without protein on pure water is essentially identical to the one on  $\text{CaCl}_2$ -containing subphase and has been omitted for clarity. A comparison of the three traces concerning the PE headgroups in Fig. 5a shows a successive shift of the phosphate stretch vibrations to higher energies in the sequence from the monolayer on water, on  $\text{Ca}^{2+}$ -containing subphase and in the protein-bound state. In contrast, the PC phosphate vibrations seem not at all affected by the addition of  $\text{Ca}^{2+}$  to the subphase (data not shown) or by protein binding. On the other hand, a major change is observed in the  $\nu_{as}(-\text{CO}-\text{O}-\text{C}-)$  vibration upon protein binding, with absorption shifted from the  $1,180 \text{ cm}^{-1}$

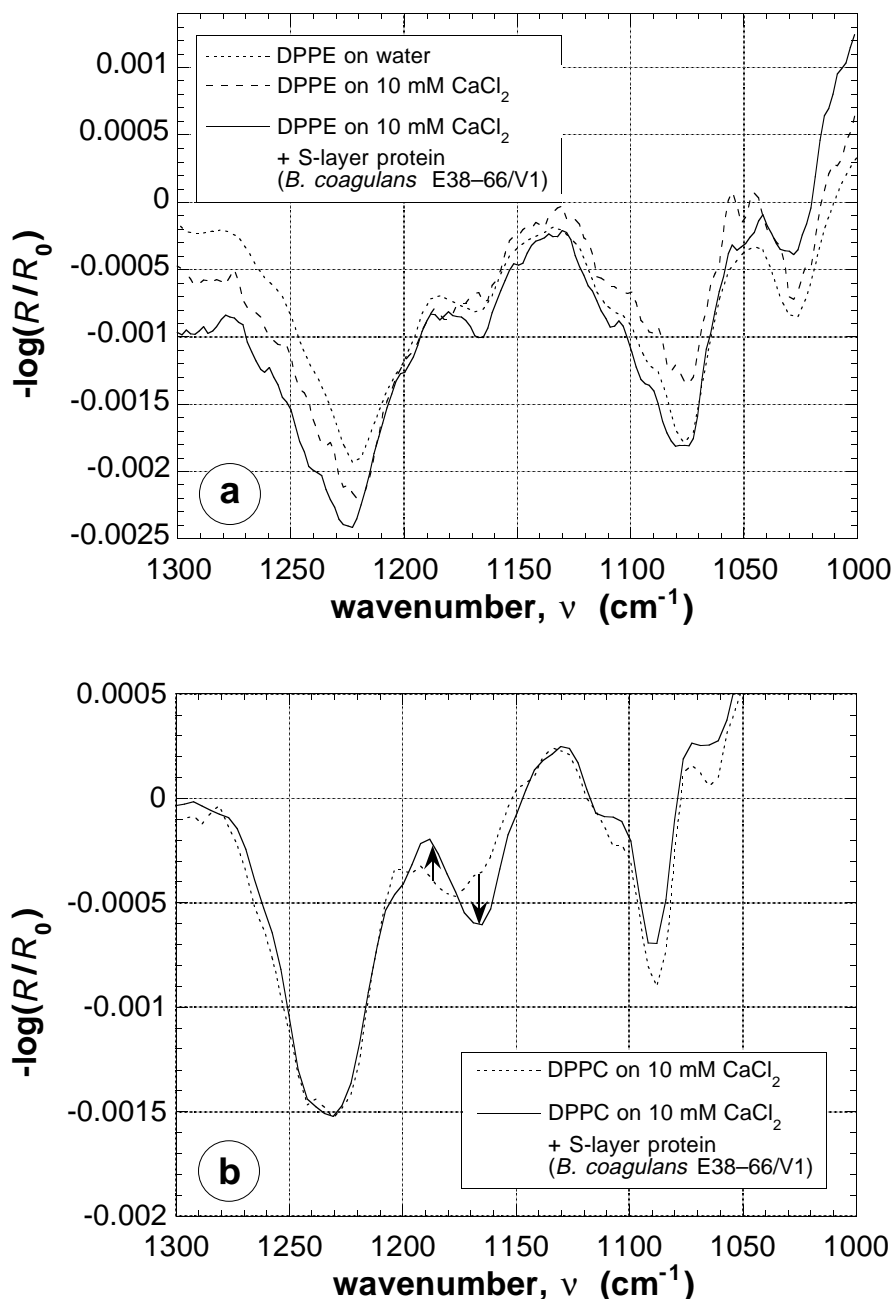


**Figure 5:**

FTIR spectra in the region of the ester carbonyl and phosphate stretch vibrations of the phospholipid headgroups.

range to about  $1,165\text{ cm}^{-1}$ . In this spectral region, the situation is not clear in the spectra taken for the PE monolayers. The most conservative conclusion that may be drawn from these data is that with PE monolayers as a recrystallization matrix, the protein interpenetrates the lipid headgroups such that the phosphate groups are affected in their molecular interactions. With PC monolayers, peptide insertion may even affect the carbonyl esters at the boundary between the hydrophilic and the hydrophobic parts of the monomolecular lipid layer. More speculative suggestions, as to what the observed spectral changes could relate to, will be put forward in the next section.

## DISCUSSION

The non-natural association of S-layer proteins from the two Gram-positive *Bacillus* species *B. coagulans* E38–66/V1 and *B. sphaericus* CCM2177 with phospholipid membranes and their recrystallization into coherent S-layer lattices bears many similarities as far as the interface between the proteins in the crystal and the lipid headgroups are concerned. Major differences have been documented between the internal structures of the S-layers.

The electron density profiles presented in Fig. 4 together with the GIXD data shown in Fig. 3 provide clear evidence that the structure of the lipid acyl chains is at best marginally affected by protein adsorption and recrystallization. In both cases studied the electron density distributions within the lipid headgroups are slightly altered. In a refined structural model of the S-protein/lipid headgroup interface within the layer system formed by the *B. sphaericus* CCM2177 protein at DPPE, derived from a simultaneous evaluation of the X-ray data with neutron reflectivity data of reconstituted S-layers under perdeuterated DPPE (DPPE- $d_{62}$ ) on  $\text{H}_2\text{O}$  and  $\text{D}_2\text{O}$ , we have specifically investigated the distribution of protein material and water within the boundary region.<sup>35</sup> We find that peptide interpenetrates deeply into the lipid headgroups – without affecting the lipid acyl chains. Concomitantly, water is introduced into the headgroup region. In view of an essentially unchanged area per lipid within the surface film, volume conservation requires that the headgroups tilt toward the surface normal to make space available for the peptide. Quantitatively, it is estimated that  $\sim 65$  electrons associated with peptide material inserts into the lipid headgroup region per lipid molecule in the monolayer. Since the coherence area within the aqueous surface which is averaged in a typical reflectivity experiment is mesoscopic, micron-sized along the projection of the beam direction on the footprint,<sup>36</sup> it is impossible to decide whether this material inserts homogeneously – on average one amino acid sidechain per lipid – or inhomogeneously – with larger peptide loops associating with only a few of

the ~ 100 DPPE molecules located within the area that one S-layer protein of the *B. sphaericus* CCM2177 variety occupies in the surface film. In view of the specificity of S-protein binding to lipids that has been revealed from systematic investigations of recrystallization conditions<sup>16</sup> it seems quite clear that the lipid headgroups interact with spatially organized peptide structures, which suggests that the latter scenario is more realistic.

While we do not have such detailed information from (neutron) reflectivity measurements available on the interface between the *B. coagulans* S-layer adhering to phospholipid headgroups, it is quite reasonable to assume that the situation there is similar. This is corroborated by the IR results shown in Fig. 5 which demonstrate that vibrational modes of the phosphates are affected by the protein in PE headgroups and that within the PC headgroups even the carbonyl esters at the boundary between the hydrophilic and the hydrophobic parts of the lipids show changes that may be associated with peptide interpenetration into the monolayer.

The molecular origin of these spectral changes is currently still a matter of debate. Generally the structure of the  $\nu_{\text{as}}(-\text{PO}_2^-)$  has been related to the hydration state of phospholipid headgroups<sup>37,38</sup> and both monolayer compression and the addition of  $\text{Ca}^{2+}$  has been implied to dehydrate PC headgroups as indicated by a shift of  $\nu_{\text{as}}(-\text{PO}_2^-)$  to higher energy.<sup>39</sup> In PE headgroups we clearly observe a shift in  $\nu_{\text{as}}(-\text{PO}_2^-)$  from 1,220 to 1,225  $\text{cm}^{-1}$  in the sequence (PE on water)  $\rightarrow$  (PE w/ 10mM  $\text{Ca}^{2+}$ )  $\rightarrow$  (PE w/  $\text{Ca}^{2+}$  and associated S-layer). This shift is of the same magnitude as has been reported for (PC on water)  $\rightarrow$  (PC w/ 5 mM  $\text{Ca}^{2+}$ ).<sup>39</sup> However, we do not observe any measurable shift in that spectral region with PC monolayers upon S-layer reconstitution (Fig. 5b). An alternative interpretation of the spectral effects in PE may thus relate the shifts to hydrogen bonding ( $-\text{NH}_3^+ \rightarrow -\text{PO}_2^-$ ) within or between the PE headgroups that might be successively disrupted by  $\text{Ca}^{2+}$  and by the insertion of peptide into the headgroups. The latter effect – the disruption of hydrogen bonds due to the insertion of peptide – would be expected as a consequence of a collective tilting of the headgroups toward the surface normal as hydrogen bonds among adjacent PE's are only formed if the ( $-\text{NH}_3^+$ ) and ( $-\text{PO}_2^-$ ) moieties are located in the same plane parallel to the interface. In that context it has also been explained by the formation of hydrogen bonds between the headgroups and their disruption by  $\text{Ca}^{2+}$  that S-layer protein do not bind and recrystallize at PE interfaces on pure water while they form well-ordered S-layers in the presence of the cation.<sup>16</sup> The model would also explain why one does not observe a similar frequency shift of the  $\nu_{\text{as}}(-\text{PO}_2^-)$  in PC as in PE upon S-layer reconstitution as PC is incapable of forming intramolecular H-bonds due to the lack of a proton donator group.

The spectral changes observed with DPPC upon S-layer protein reconstitution in the region between 1,150 and 1,200  $\text{cm}^{-1}$  is associated with conformational changes of the glycerol backbone. The  $\nu_{as}(-\text{CO}-\text{O}-\text{C}-)$ , which gives rise to adsorption in this region, is centered around 1,165 or 1,180  $\text{cm}^{-1}$ , depending on whether the  $(-\text{CO}-\text{O}-\text{C}-)$  fragment is oriented more normal or more parallel to the interface.<sup>37</sup> In lipid crystals<sup>40</sup> as well as in model membranes,<sup>41</sup> the linker fragment of the acyl chain at the  $\beta$  position is preferentially oriented along the surface normal, whereas at the  $\alpha$  position it is oriented parallel before the chain turns and points away from the interface. This is presumably also true in the DPPC monolayer on  $\text{Ca}^{2+}$ -containing subphase (trace 1 in Fig. 5b), where the spectral intensity is rather uniformly distributed between the 1,165 and the 1,180  $\text{cm}^{-1}$  positions. In contrast, upon S-layer reconstitution we observe a redistribution of the absorption from 1,180 to the 1,165  $\text{cm}^{-1}$  (see arrows in Fig. 5b), which may be indicative of a conformational change of the linker fragment at the  $\beta$  position into an orientation more parallel to the interface. Whether this change is a direct or indirect consequence of peptide insertion into the headgroup is not clear; it should be noted, however, that similar spectral differences may also be observed between DPPC monolayers that have been compressed with greatly differing barrier speeds (M. Schalke, unpublished results). As the spectra in Fig. 5 have been obtained under comparable preparation conditions with respect to the lipid monolayer we infer from these results that the peptide material from the S-layer inserts deeply into the PC moiety leading to a gross reorganization of the lipid headgroups.

Both GIXD and reflectometry reveal major differences in the internal structure of the S-layer between the two protein species. This is not too surprising since the two proteins have significantly different molecular weights ( $M_r \sim 100,000$  and  $120,000$  for the *B. coagulans* and the *B. sphaericus* proteins, respectively) and amino acid composition. Whereas the S-layer of *B. sphaericus* has a square lattice, that of *B. coagulans* has a lattice of oblique symmetry. In addition, the protein density distribution across the S-layer is characteristically different for the two proteins: While the *B. sphaericus* S-layer has two distinct density maxima with a pronounced minimum in between, and has a layer thickness in excess of 90 Å,<sup>12</sup> the *B. coagulans* protein density distribution exhibits just one hump, which is located close to the lipid monolayer, and extends only  $\sim 40$  Å along the  $z$  direction. This indicates a lipid/protein layer structure, shown schematically in Fig. 6, which is quite different from that of the *B. sphaericus* S-layer (compare with Fig. 6 in ref. 12). Integration over the electron density distribution yields estimates of the partial volume of the protein and the number of electrons associated with the

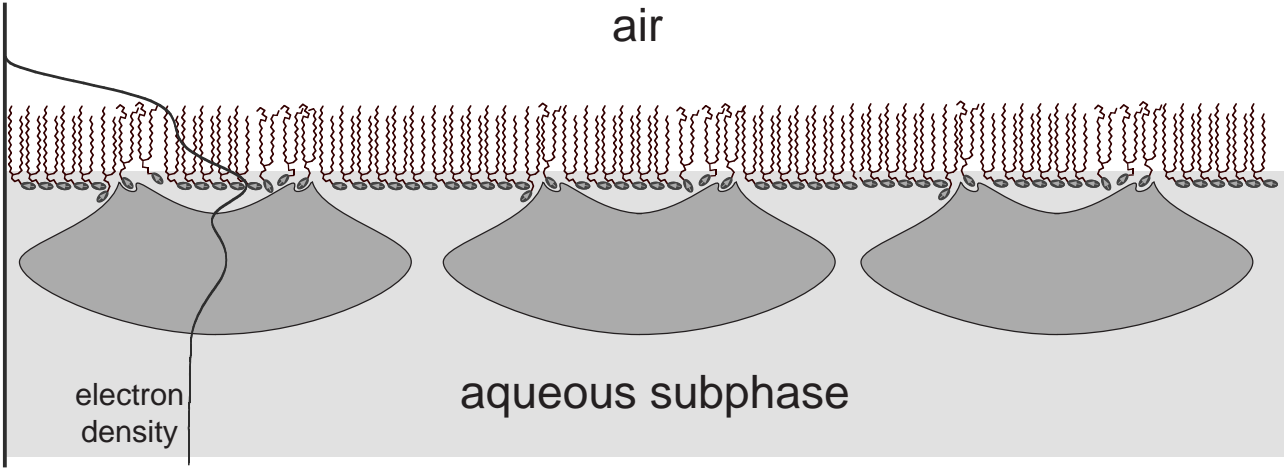


**Figure 6:**

Cartoon of the lipid/protein multilayer structure for S-layer protein from *B. coagulans* E38–66/V1 as it emerges from the analysis of the electron density profile, indicated on the left-hand side. The appearance of the protein is consistent with the electron density profile, and proteins and lipids are approximately to scale. There is, however, no structural information for the protein available to date on the atomic scale.

protein per unit area. Let  $\rho_{lipid}(z)$  be the electron density profile of the lipid-only system (dashed line in Fig. 4b) and  $\rho(z)$  the electron density profile of the lipid/protein system (full line in Fig. 4b). Then we may estimate the distribution of protein volume fraction  $\xi_{pr}(z)$  as

$$\xi_{pr}(z) = \frac{\rho(z) - \rho_{lipid}(z)}{\rho_{pr} - \rho_{lipid}(z)} \quad (4),$$

where  $\rho_{pr}$  is the average electron density of protein dry matter. Using the amino acid composition of the protein<sup>42</sup> in connection with data for the partial volumes of amino acids in crystals<sup>43</sup> and a correction for the packing efficiency of peptides in proteins<sup>23,44</sup> we estimate  $\rho_{pr} \sim 0.4268 \text{ e}^- \text{ \AA}^{-3}$ . Then

$$V_{pr} = \int_{\text{interface}} \xi_{pr}(z) dz \cdot A_{\text{unit cell}} \quad (5)$$

evaluates to a dry volume,  $V_{pr} \sim 110,000 \text{ \AA}^3$  (per unit cell size) and the number of electrons,

$$n_e^{pr} = \rho_{pr} \cdot V_{pr} \quad (6)$$

yields  $n_e^{pr} \sim 47,000$ . In comparison, converting the amino acid composition directly into the number of electrons and the volume expected per protein monomer results in  $n_e^{E38\pm66} \sim 50,700$  and  $V_{E38-66} \sim 118,700 \text{ \AA}^3$ . This estimate provides an important consistency check on the evaluation procedure and shows that one morphological unit is contained within the unit cell area,  $A_{\text{unit cell}} \sim 7,500 \text{ \AA}^2$ . The latter result has been also derived from EM characterization of the S-layers.<sup>9</sup>

## CONCLUSIONS

The motivation for this paper has two major components: (a) to summarize the molecular details of the coupling of the S-layer protein from, specifically, *B. coagulans* E38–66/V1 to phospholipid monolayers and to compare these details with the data – published earlier<sup>12</sup> – for the protein from *B. sphaericus* CCM2177 and (b) to review the state of the art in surface sensitive structure characterization techniques at the air/water interface that have been used to reveal this information. As regards the former of these goals it has been shown that the molecular details of the coupling, at the level of the protein/lipid interface, are quite similar for the two protein species although the protein structure – and hence the S-layer structure – seem rather different. On the experimental side, the methods applied for the structural characterization of S-layers coupled to lipid surface monolayers are not restricted to large proteins, such as the S-layer proteins investigated, but are quite general: Peptides, pharmaceuticals, glycopolymers, glycosylated surfactants, or nucleic acids are all interesting systems that will lend themselves for similar investigations of their respective interactions with model membranes. There have been three major developments within the recent past: (i) GIXD measurements of monomolecular protein sheet crystals anchored at the air-water interface have become feasible<sup>45</sup> and have been further developed to become an ever more powerful tool of surface characterization.<sup>12,46</sup> (ii) X-ray reflectivity measurements are boosted by the increased brilliance of modern Synchrotron radiation sources and – to a lesser extent – of technical improvements of laboratory scale X-ray sources;<sup>12,22</sup> at the same time, contrast variation with neutron reflection experiments and composition-refinement techniques for data evaluation,<sup>23,35,47</sup> as well as model-free data inversion techniques<sup>24</sup> and high-resolution models of lipid monolayers<sup>48</sup> are taking advantage of such performance improvements. (iii) Finally, the FT-IRRAS technique for the investigation of monomolecular surface layers on aqueous subphases has taken the step beyond methylene spectroscopy of alkyl or acyl chains at the interface and has matured into a stable and ultra-sensitive technique for probing the molecular environment of specific molecular fragments within molecular surface architectures, yielding new insights both in life science and materials science.<sup>32,49-51</sup> We have shown in this paper that the combination of these powerful methods enable the discussion of the structure of organic interface layers in molecular detail.

## ACKNOWLEDGMENTS

We thank Jan Skov Pedersen (JSP) for making available to us his program for form-free fitting of reflectivities<sup>24</sup> and JSP and Michael Gerstenberg for helpful advice. We are grateful to HASYLAB at DESY, Hamburg, for beamtime at the intense beamline BW1<sup>21</sup> of the DORIS bypass. This work has been supported by the German Science Foundation (SFB 294, TP C10), the Austrian Science Foundation (projects S7204/S7205), the Fonds der Chemischen Industrie, Frankfurt, the Danish Dansync programme, and the EC-TMR (contract no. ERBFMGECT950059).

## REFERENCES

- 1 A. Diederich and M. Lösche, in: *Protein array: An alternate biomolecular system*, ed. K. Nagayama, Japan Scientific Societies Press/Elsevier, Tokyo/Limerick, 1997, p. 205
- 2 Y. Lvov, K. Ariga, I. Ichinose and T. Kunitake, *J. Am. Chem. Soc.*, 1995, **117**, 6117.
- 3 W. Knoll, M. Liley, D. Piscevic, J. Spinke and M. J. Tarlov, in: *Protein array: An alternate biomolecular system*, ed. K. Nagayama, Japan Scientific Societies Press/Elsevier, Tokyo/Limerick, 1997, p. 231
- 4 M. Lösche, *Curr. Opin. Solid State Mats. Sci.*, 1997, **2**, 546.
- 5 E. Sackmann, *Science*, 1996, **271**, 43.
- 6 U. B. Sleytr, P. Messner, D. Pum and M. Sára, *Angew. Chem. Int. Ed. Engl.*, 1999, **38**, 1034.
- 7 *Crystalline Bacterial Cell Surface Proteins*, ed. U. B. Sleytr, P. Messner, D. Pum and M. Sára, Academic Press, San Diego/Austin, 1996
- 8 U. B. Sleytr and T. J. Beveridge, *Trends Microbiol.*, 1999, **7**, 253.
- 9 D. Pum, M. Sára and U. B. Sleytr, *J. Bacteriol.*, 1989, **171**, 5296.
- 10 P. Messner and U. B. Sleytr, *Adv. Microbiol. Physiol.*, 1992, **33**, 213.
- 11 M. Sára and U. B. Sleytr, *Progr. Biophys. Molec. Biol.*, 1996, **65**, 83.
- 12 M. Weygand, B. Wetzer, D. Pum, U. B. Sleytr, K. Kjaer, P. B. Howes and M. Lösche, *Biophys. J.*, 1999, **76**, 458.
- 13 D. Pum and U. B. Sleytr, *Trends Biotechnol.*, 1999, **17**, 8.
- 14 D. Pum, M. Weinhandl, C. Hödl and U. B. Sleytr, *J. Bacteriol.*, 1993, **175**, 2762.
- 15 D. Pum and U. B. Sleytr, *Thin Solid Films*, 1994, **244**, 882.

- 16 B. Wetzer, A. Pfandler, E. Györvary, D. Pum, M. Lösche and U. B. Sleytr, *Langmuir*, 1998, **14**, 6899.
- 17 B. Schuster, D. Pum and U. B. Sleytr, *Biochim. Biophys. Acta*, 1998, **1369**, 51.
- 18 B. Schuster, D. Pum, O. Braha, H. Bayley and U. B. Sleytr, *Biochim. Biophys. Acta*, 1998, **1370**, 280.
- 19 U. B. Sleytr, M. Sára, S. Küpcü and P. Messner, *Arch. Microbiol.*, 1986, **146**, 19.
- 20 A. Diederich, C. Sponer, D. Pum, U. B. Sleytr and M. Lösche, *Colloids Surf. B: Biointerf.*, 1996, **6**, 335.
- 21 R. Frahm, J. Weigelt, G. Meyer and G. Materlik, *Rev. Sci. Instrum.*, 1995, **66**, 1677.
- 22 P. Krüger, M. Schalke, T. Gutberlet and M. Lösche, *Rev. Sci. Instrum.*, 1999, in preparation.
- 23 M. Lösche, M. Piepenstock, A. Diederich, T. Grünwald, K. Kjaer and D. Vaknin, *Biophys. J.*, 1993, **65**, 2160.
- 24 J. Skov Pedersen and I. W. Hamley, *Physica B*, 1994, **198**, 16.
- 25 I. W. Hamley and J. Skov Pedersen, *J. Appl. Cryst.*, 1994, **27**, 29.
- 26 J. Skov Pedersen and I. W. Hamley, *J. Appl. Cryst.*, 1994, **27**, 36.
- 27 J. Als-Nielsen and K. Kjaer, in: *Phase Transitions in Soft Condensed Matter*, ed. T. Riste and D. Sherrington, Plenum Press, New York, 1989, p. 113
- 28 J. Als-Nielsen, D. Jacquemain, K. Kjaer, M. Lahav, F. Leveiller and L. Leiserowitz, *Phys. Rep.*, 1994, **246**, 251.
- 29 G. H. Vineyard, *Phys. Rev. B*, 1982, **26**, 4146.
- 30 K. Kjaer, *Physica B*, 1994, **198**, 100.
- 31 R. A. Dluhy and D. G. Cornell, *J. Phys. Chem.*, 1985, **89**, 3195.
- 32 R. Mendelsohn, J. W. Brauner and A. Gericke, *Annu. Rev. Phys. Chem.*, 1995, **46**, 305.
- 33 C. R. Flach, A. Gericke and R. Mendelsohn, *J. Phys. Chem.*, 1997, **101**, 58.
- 34 D. A. Cadenhead, F. Müller-Landau and B. M. J. Kellner, in: *Ordering in Two Dimensions*, ed. S. K. Sinha, Elsevier North Holland, Amsterdam, 1980, p. 73
- 35 M. Weygand, B. Wetzer, D. Pum, U. B. Sleytr, P. B. Howes, K. Kjaer and M. Lösche, 1999, in preparation.
- 36 D. Vaknin, J. Als-Nielsen, M. Piepenstock and M. Lösche, *Biophys. J.*, 1991, **60**, 1545.

- 37 U. P. Fringeli and H. H. Günthard, in: *Membrane Spectroscopy*, ed. E. Grell, Springer, New York, 1981, p. 270
- 38 R. A. Dluhy, D. G. Cameron, H. H. Mantsch and R. Mendelsohn, *Biochemistry*, 1983, **22**, 6318.
- 39 C. R. Flach, J. W. Brauner and R. Mendelsohn, *Biophys. J.*, 1993, **65**, 1994.
- 40 H. Hauser, I. Pascher, R. H. Pearson and S. Sundell, *Biochim. Biophys. Acta*, 1981, **650**, 21.
- 41 G. Cevc and D. Marsh, *Phospholipid Bilayers. Physical Principles and Models*, Wiley-Interscience, New York, 1987
- 42 M. Sára, personal communication
- 43 S. J. Perkins, in: *Modern Physical Methods in Biochemistry, Part B*, ed. A. Neuberger and L. L. M. V. Deenen, Elsevier, Amsterdam, 1988, p. 143
- 44 M. Lösche, Habilitationsschrift [in German], Mainz University (1994)
- 45 H. Haas, G. Brezesinski and H. Möhwald, *Biophys. J.*, 1995, **68**, 312.
- 46 S. A. W. Verclas, P. B. Howes, K. Kjaer, A. Wurlitzer, M. Weygand, G. Büldt, N. A. Dencher and M. Lösche, *J. Mol. Biol.*, 1999, **287**, 837.
- 47 D. Vaknin, K. Kjaer, J. Als-Nielsen and M. Lösche, *Biophys. J.*, 1991, **59**, 1325.
- 48 M. Schalke, P. Krüger, M. Weygand and M. Lösche, *Biochim. Biophys. Acta*, 1999, accepted for publication.
- 49 A. Gericke, C. R. Flach and R. Mendelsohn, *Biophys. J.*, 1997, **73**, 492.
- 50 C. R. Flach, A. Gericke, K. M. W. Keough and R. Mendelsohn, *Biochim. Biophys. Acta*, 1999, **1416**, 11.
- 51 M. Schalke, J. Friedmann, U. B. Sleytr and M. Lösche, 1999, in preparation.